XLVI CILAMCE
2025

# TUNSET: A machine learning tool for predicting tunnel settlement

Gustavo de Oliveira Daumas[1], Dimas Betioli Ribeiro[1],José Geraldo de Araújo Silva[2].

[1]*Civil Engineering Division, Aeronautics Institute of Technology*
*Praça Marechal Eduardo Gomes, 12228-900, São Paulo/São José dos Campos, Brazil*
*dimasbetioli@gmail.com*
[2]*Materials Research Division, Federal University of Ouro Preto*
*Campus Morro do Cruzeiro, 35.400-000, Minas Gerais/Ouro Preto, Brazil*
*jgaraujo@gmail.com*

**Abstract.** Urban tunneling demands reliable, uncertainty-aware settlement predictions at low computational cost. This work develops and validates two machine-learning metamodels, Random Forest (RF) and Gradient Boosting (GB), trained on staged finite-element simulations in ADONIS of Sequential Tunnel Excavation with SPT-informed strata. The surrogates emulate displacements and, through quantile objectives (GB) and quantile regression forests (RF), provide prediction intervals that support risk-informed design. On a legacy dataset, both metamodels achieve near-perfect point accuracy ($R^2 = 0.999$, RMSE $\approx 8.2$ to $8.7 \times 10^{-7}$ m; rank correlation $\geq 0.995$). GB attains empirical 95% coverage close to nominal (93%), whereas RF under-covers (83%) with narrower intervals. Leveraging millisecond-level inference cost, we perform Monte Carlo analyses with up to $10^4$ realizations to estimate failure probability and to prioritize additional site investigation where residual uncertainty is most influential. The approach markedly reduces the number of finite-element solves and can curtail costly geotechnical testing along long alignments. Overall, the pipeline from SPT-based parameterization to finite-element simulation, surrogate training, and uncertainty propagation provides traceable, near real-time predictions suitable for design screening and transparent communication of risk in geotechnical tunneling.

**Keywords:** Metamodels, Random Forest, Gradient Boosting, Sequential Tunnel Excavation, Monte Carlo.

## 1 Introduction

Integrating machine learning (ML) techniques has facilitated significant advancements in the modelling and analysis of underground structures, enabling various studies to explore computational tools for prediction. These span purely mathematical developments to broader engineering applications Adeli and Yeh [1], McKay et al. [2], Abueidda et al. [3], Bai et al. [4], including specialized approaches in geotechnical engineering and tunnels Yilmaz and Sendir [5], Hellmich et al. [6], Lackner et al. [7]. Recently, Xu et al. [8] underscored the effectiveness of multi-fidelity operator learning in predicting displacement fields of tunnel linings under diverse load conditions using a mix of low- and high-fidelity monitoring data. Additionally, Zhang et al. [9], Zhou et al. [10] advanced the state of the art by extracting internal forces and identifying cracks in tunnel linings.

Concurrently, Wang et al. [11] proposed SL-PINN, a physics-informed neural network for estimating tunnel-lining loads in elastic soils, and operator-learning schemes have been explored to infer tunnel displacement fields from multi-fidelity data Xu et al. [8]. In this paper, such PINN and operator-learning approaches are cited solely to frame the state of the art; they are neither implemented nor evaluated here.

Beyond algorithmic choices, uncertainty modelling is central in geomechanics. At the lumped scale, *random variables* (RVs) represent layer-wise constants (e.g., $E$, $c$, $\varphi$, $\nu$) with prescribed marginals and, optionally, cross-correlations, enabling efficient Monte Carlo simulation, as adopted in this work. At the spatial scale, *random fields* (RFs) capture pointwise variability and correlation of soil properties, with correlation lengths controlling scale-of-fluctuation effects and potentially altering failure mechanisms and probabilities compared with RV-only models; see, e.g., Siacara et al. [12] for RF-driven reliability in FEM slope analyses and classic treatments in Phoon and Kulhawy [13], Fenton and Griffiths [14]. While we focus on an RV framework for scalability, the surrogate paradigm extends naturally to RFs by parameterizing a low-dimensional set of field modes (e.g., Karhunen–Loève coefficients) as inputs to the surrogate.

In line with this perspective, we adopt a purely data-driven surrogate strategy and assess two ensemble regressors: a Random Forest (RF) and a Gradient Boosting (GB) metamodel, both calibrated on a large ensemble of ADONIS finite-element simulations (Section 2.2). These surrogates emulate the FE responses with high fidelity, maintain low computational overhead for training and inference, and enable large-scale Monte Carlo analyses

with up to $10^4$ realizations to estimate failure probability under input uncertainty. The integration of calibrated FE-based surrogates with uncertainty propagation enhances scientific rigor and practical applicability for complex geotechnical scenarios.

This paper develops and validates data-driven surrogates for predicting tunnel-induced ground settlements, calibrated on staged finite-element simulations (ADONIS) with SPT-informed strata. The goal is to deliver fast, uncertainty-aware predictions suitable for design screening while preserving traceability to the layered geotechnical model.

## 2 SPT correlations

In the development of a geotechnical model for soil behaviour analysis, particularly in contexts where detailed in-situ test data are scarce or non-existent, the correlations between the N-value of the Standard Penetration Test (NSPT) and the mechanical properties of the soil play a critical role. According to Kumar et al. [15], empirical correlations between the NSPT and cohesion, internal friction angle, dilation angle (assumed equal to the internal friction angle for simplification), and Poisson's ratio provide a robust basis for the preliminary analysis required in many geotechnical engineering projects.

Soil cohesion, which measures its ability to resist shearing without confinement, can be estimated through correlations that directly link these mechanical properties with the NSPT. These correlations benefit cohesive and intermediate soils, where cohesion varies significantly with compaction and soil moisture. Kumar et al. [16] offer a specific formulation that adjusts cohesion based on the NSPT, allowing predictions that align well with experimental observations.

The internal friction angle, describing soil resistance to sliding, also correlates with the NSPT. This property is fundamental for the design of slopes, foundations, and other retaining structures. The study by Kumar et al. [16] suggests that the internal friction angle can be directly inferred from the NSPT, simplifying the modelling of soil shear resistance without requiring extensive laboratory tests.

In many soil stability analyses, the dilation angle, which directly impacts the material's plastic zone, is often assumed to be equal to the friction angle and treated similarly. This assumption simplifies the modelling process by assuming the soil's volumetric behaviour during shearing is proportional to its shear strength.

Finally, Poisson's ratio, which describes the relationship between transverse and axial deformation when the soil is subject to stress, is another property that can be estimated indirectly through the NSPT. A simple relationship between the shear modulus (G) and the modulus of elasticity (K) (Eq. 1), or through an empirical formula presented in Kumar et al. [15] (Eq. 2), facilitates understanding the deformation characteristics of soil under loads.

$$\nu = \frac{3K - 2G}{2(3K + G)}, \tag{1}$$

where $K$ denotes the bulk modulus and $G$ the shear modulus.

$$\nu = 0.20 + 0.01\,N, \tag{2}$$

where $N$ is the SPT $N$-value (blows/30 cm).

Corresponding to (2.22) we have, for the special Lagrangian (1.6):

$$p_j = a_{hj}\dot{x}^h,$$

the counterpart of (2.23) being

$$^j = a^{jh}p_h.$$

Below is the Python routine programmed to extract parameters of interest with just the insertion of the NSPT value:

```python
def soil_prop(N):
    # shear modulus G [Pa]
    G = 1000 * 325 * (N ** 0.68) * 47.880258888889
    # bulk modulus K [Pa]
    K = 1000 * 700 * N / (3 * (1 - 2 * (0.2 + 0.005 * N)))
    if N < 30:
        c = 1000 * (-16.5 + 2.15 * N)  # cohesion c [Pa]
    else:
        c = 48000                      # cohesion c [Pa] for high SPT values
    phi = 27.12 + 0.285 * N            # friction angle    [deg]
```

```
    return G, K, c, phi
```

Listing 1. Calculation of Soil Properties Based on SPT N value

When integrated into geotechnical models, these correlations enable engineers and designers to make quick and reliable estimates of soil properties, which is essential for the safe design and analysis of geotechnical structures. The application of these empirical correlations not only saves significant time and resources and enhances the reliability of geotechnical analyses in projects where detailed test data are limited.

To test and validate the model, this study utilized the following Standard Penetration Test (SPT) data, Table 1, which was subsequently used to calculate the average soil parameters.

Table 1. SPT (N–value) along depth.

| **Depth (m)** | 5 | 6 | 7 | 8 | 9 | 11 | 13 | 18 | 20 | 22 | 25 | 26 | 28 | 30 | 32 | 34 | 36 | 38 | 40 |
|---|---|---|---|---|---|---|---|---|---|---|---|---|---|---|---|---|---|---|---|
| **SPT (blows/30 cm)** | 7 | 36 | 27 | 18 | 20 | 23 | 27 | 26 | 29 | 42 | 39 | 44 | 41 | 43 | 37 | 37 | 39 | 41 | 41 |

### 2.1 ADONIS model

The two-dimensional analyses were carried out in ADONIS under plane-strain conditions to represent the interaction between the tunnel lining and the surrounding ground. The soil domain was partitioned into horizontal strata consistent with the SPT profile (Table 1). Each stratum was assigned Mohr–Coulomb parameters $(\rho, \varphi, c)$ mapped from the corresponding NSPT intervals, while the elastic constants were specified globally as shear modulus $G$ and bulk modulus $K$; dilation was taken as $\psi = \varphi$. The lining, idealized as a circular arch, was modeled with curved Euler–Bernoulli beam elements. The ground was discretized with linear three-node triangles (T3) generated via `gmsh` with a target maximum edge length of $1.0$ m, as illustrated in Fig. 1.

Far-field boundary conditions were applied to prevent spurious rigid-body motions and boundary effects: horizontal displacements were constrained to zero at the two vertical boundaries, and both horizontal and vertical displacements were fixed at the model base to emulate a stiff rock horizon. The initial geostatic stress state $(\sigma_{yy}, \sigma_{xx}, \sigma_{zz})$ was computed from self-weight using layer densities and gravity, with lateral stresses obtained from layer-wise at-rest coefficients $K_0 = \{0.50,\ 0.60,\ 0.65\}$. An excerpt of the initialization script used in ADONIS is shown in Listing 2.

```
var grav = 9.81
var dsyy1 = 1950*grav
var isyy1 = 0.0
var dsyy2 = 2200*grav
var isyy2 = dsyy2*4.0 - dsyy1*4.0
var dsyy3 = 2400*grav
var isyy3 = dsyy3*(4.0+12.0) - dsyy1*4.0 - dsyy2*12.0
var dsyy4 = 2600*grav
var isyy4 = dsyy3*(4.0+12.0+20) - dsyy1*4.0 - dsyy2*12.0 - dsyy3*20.0
var k01 = 0.5
var k02 = 0.6
var k03 = 0.65
var k04 = 0.65
```

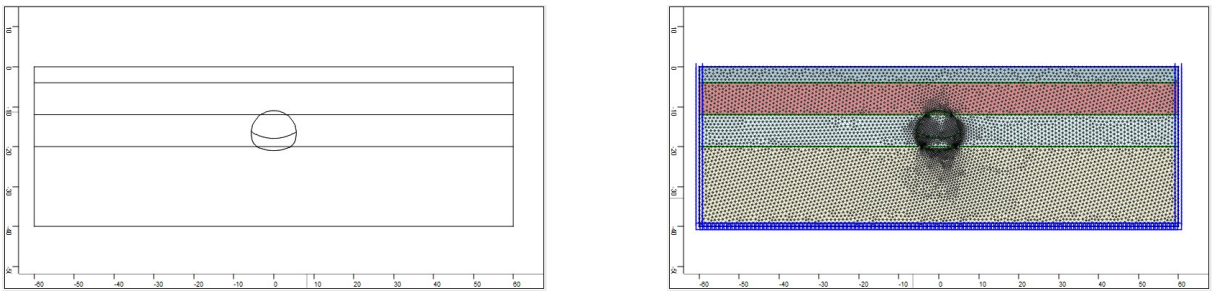
Listing 2. Initialization of geostatic stresses in ADONIS.

A staged-construction procedure was adopted to mimic the excavation sequence and the associated nonlinearity of the ground response. First, the top heading was excavated across the upper two strata; during this phase, a $60\%$ stress relaxation was applied to represent the transient unloading immediately after excavation. Temporary support (shotcrete arch) was then installed and the system re-equilibrated. Next, the bench was excavated and the lining completed, followed by a final static solution to assess equilibrium, displacements, and internal forces (see Fig. 2).

A Python pre-processor automated (i) the conversion of SPT data into layer properties, (ii) the generation of ADONIS input blocks (geometry, mesh, constitutive and stage commands), (iii) the execution of analyses, and (iv) the structured storage of outputs for post-processing and metamodel training. In the stochastic campaign (1000 realizations), the pre-processor perturbed the material parameters around their layer-wise means according to a common statistical law. Specifically, all continuously varied parameters were sampled as

$$X \sim \mathrm{TN}(\mu, \sigma), \qquad \sigma = 0.01\,\mu, \qquad X \in [\,\mu - 0.02\,\mu,\ \mu + 0.02\,\mu\,],$$

[0]Terzaghi, K. and Peck, R. B.(1967)Terzaghi and Peck [17]. Kumar et al(2014,2015,2016)Kumar et al. [15]Kumar et al. [18]Kumar et al. [19].



(a) Tunnel geometry (b) Finite element mesh (T3)

Figure 1. Model configuration and boundary conditions.

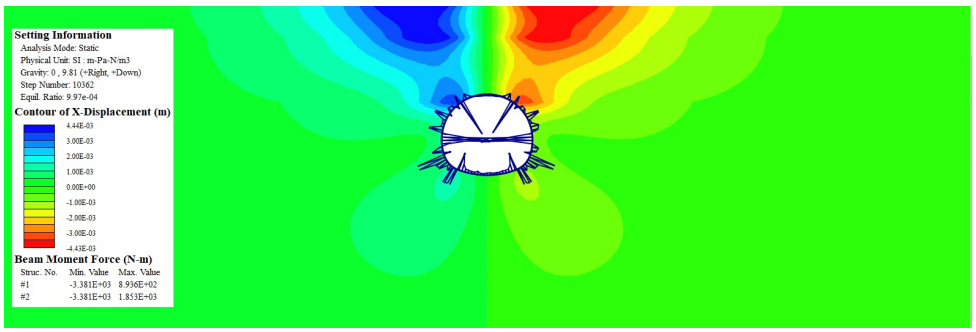



Figure 2. Vertical ground displacement and bending moment in the lining.

which yields a nominal coefficient of variation of $1\%$; because of the symmetric truncation at $\pm 2\sigma$, the effective standard deviation is $\sigma_{\text{eff}} \approx 0.8796\,\sigma$ (effective CoV $\approx 0.88\%$). This distribution was applied uniformly to $\rho$, $\varphi$, $\psi(=\varphi)$, $c$, $G$, and $K$. The layer-wise mean properties for the three clay strata (mapped from NSPT ranges) are summarized in Table 2, and the global elastic moduli in Table 3. All strengths and stresses were entered in ADONIS in pascals.

Table 2. Layer-wise mean geotechnical properties (clay).

| Layer | NSPT (blows/30 cm) | Density $\rho$ (kg/m$^3$) | Friction $\varphi$ (deg) | Cohesion $c$ (kPa) |
|---|---|---|---|---|
| 1 | 10–30 | 1800 | 22 | 40 |
| 2 | 30–50 | 1900 | 25 | 45 |
| 3 | 30–50 | 1900 | 25 | 45 |

Notes: dilation $\psi = \varphi$ (same mean and dispersion). In ADONIS inputs, $c = 4.0 \times 10^4$ Pa (Layer 1) and $4.5 \times 10^4$ Pa (Layers 2–3).

Table 3. Global elastic moduli and dispersion.

| Parameter | Unit | Mean $\mu$ | Nominal $\sigma$ $(= 1\%\mu)$ | Truncation $(\pm 2\%)$ |
|---|---|---|---|---|
| Shear modulus $G$ | Pa | $2.80 \times 10^9$ | $2.80 \times 10^7$ | [2.744e9, 2.856e9] |
| Bulk modulus $K$ | Pa | $3.90 \times 10^9$ | $3.90 \times 10^7$ | [3.822e9, 3.978e9] |

The implied mean Poisson's ratio is $\nu = \frac{3K-2G}{2(3K+G)} \approx 0.21$. Under the same truncation, the effective CoV for $G$ and $K$ is also $\approx 0.88\%$.

## 2.2 Random Forest and Gradient Boosting

Random Forest is an ensemble learning algorithm based on the combination of multiple decision trees to improve predictive performance and reduce overfitting. Each decision tree in the ensemble is constructed from a different bootstrap sample of the original dataset and follows a recursive partitioning process starting from a root node. At each node, a random subset of input features is selected, and the optimal split is determined based on a

predefined criterion, typically mean squared error (MSE) for regression tasks. The tree is grown until a stopping condition is met, such as a maximum depth or a minimum number of samples per leaf.

Unlike a single decision tree, which is prone to high variance and overfitting, the Random Forest algorithm mitigates this issue by aggregating the predictions of many uncorrelated trees. The final output is computed as the average of the predictions from all trees in the ensemble, leveraging the law of large numbers to stabilize and improve generalization. This approach benefits from the combination of bagging (bootstrap aggregation) and random feature selection, making Random Forest a robust and versatile method for handling high-dimensional, nonlinear regression problems Ho [20].

Gradient Boosting is a complementary ensemble technique that builds a strong predictor by adding shallow decision trees sequentially, each one trained to reduce the residual errors of the current model. In the regression setting, the procedure fits a new tree to the negative gradient of the loss with respect to the current predictions, most commonly the squared error, and updates the model with a shrunken step controlled by the learning rate. Model capacity is governed by the number of estimators and by the complexity of each base learner, which is typically limited by small depth and minimum samples per leaf in order to act as weak learners.

Regularization plays a central role in Gradient Boosting. Shrinkage through a small learning rate improves generalization, subsampling a fraction of the data at each boosting stage introduces stochasticity that reduces variance, and early stopping on a validation split prevents overfitting once the validation loss ceases to improve. In practice, Gradient Boosting tends to capture smooth additive and interaction effects with high accuracy under careful hyperparameter tuning, offering a strong alternative to Random Forest when fine control of bias–variance trade-offs and predictive intervals via quantile objectives are desired.

### 2.3 Results: predictive accuracy and uncertainty

We assessed two surrogates on the legacy dataset used at the time of writing: (i) Gradient Boosting with 5-fold cross-validation (GB) and (ii) Random Forest (RF) with empirical 95% prediction intervals from the distribution of tree outputs. Figure 3 shows parity plots comparing simulated (ADONIS) responses against metamodel predictions; Table 4 summarizes the main metrics.

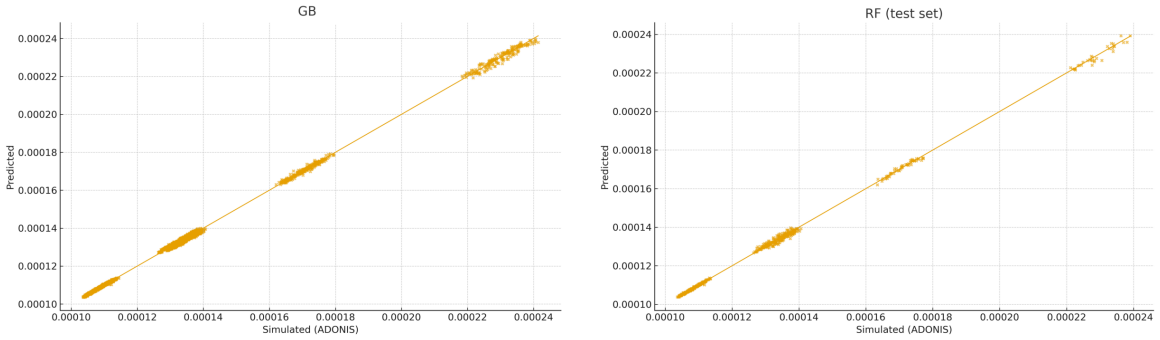



Figure 3. Parity plots (legacy dataset): predicted vs. simulated (ADONIS) responses with 1:1 line. Left: GB. Right: RF (test set).

Table 4. Model performance on the legacy dataset. Coverage95% is the fraction of true values within the nominal 95% prediction interval; Avg. width is the mean interval width.

| Model | $R^2$ | RMSE (m) | MAE (m) | Spearman | Coverage95% | Avg. width (m) |
|---|---|---|---|---|---|---|
| GB | 0.999 | 8.20e-07 | 6.21e-07 | 0.996 | 93.0% | 2.91e-06 |
| RF (test set) | 0.999 | 8.73e-07 | 5.75e-07 | 0.995 | 83.0% | 1.90e-06 |

Both models achieve near-perfect point accuracy ($R^2 = 0.999$) with very small errors (RMSE $\sim 8.2-8.7 \times 10^{-7}$ m). In terms of uncertainty, GBattains coverage close to nominal (93% vs. 95% target), whereas RF under-covers (83%) with narrower average intervals (about $1.9 \times 10^{-6}$ m vs. $2.9 \times 10^{-6}$ m for GB).

## 3 Conclusions

We coupled ADONIS-based simulations of Sequential Tunnel Excavation (SEM) with machine-learning metamodels to enable rapid predictions of soil–tunnel responses and uncertainty quantification ready to support engineering decisions. On the legacy dataset, both the gradient-boosting (GB) metamodel and the Random Forest (RF) metamodel yield essentially indistinguishable point predictions, achieving $R^2 = 0.999$ with sub-micrometer errors (RMSE $\approx$ 8.2–8.7 $\times 10^{-7}$ m) and rank correlation $\geq 0.995$, thereby preserving the ordering of scenarios. The key difference lies in probabilistic calibration: as summarized in Table 4, GB attains empirical coverage close to nominal for 95% prediction intervals (93%), whereas RF tends to under-cover (83%) because it produces tighter intervals. For preliminary scenario screening and transparent communication of uncertainty to engineers, project managers, and regulatory bodies, calibrated intervals are preferable; for ranking alternatives under tight computational budgets, narrower bands may be used provided that an explicit safety margin is adopted.

From an engineering standpoint, residuals well below $10^{-6}$ m are orders of magnitude smaller than typical serviceability-limit displacements on the order of $10^{-3}$ m. This supports replacing numerous finite-element (FE) evaluations in sensitivity analyses and parametric studies without compromising practical conclusions. Adopting probabilistic modeling with prediction intervals and coverage metrics also allows the reduction of extensive geotechnical investigation campaigns: for long tunnels, the number of boreholes and tests can easily reach hundreds or even thousands, depending on alignment length and ground heterogeneity. A well-calibrated metamodel, combined with *in situ* monitoring, enables prioritization of additional boreholes and laboratory tests only where residual uncertainty materially affects project risk, thereby optimizing cost and schedule.

Another advantage is practical applicability. While a typical FE model may require hours per run under realistic conditions, a trained machine-learning model returns answers in fractions of a second, enabling near real-time screening, scenario exploration, iterative optimization, and rapid decision updates during design. This speedup markedly reduces computational cost per iteration and frees FE resources for targeted reanalyses in critical situations.

In practical use, a serviceability threshold $\Delta_{\text{lim}}$ is defined for vertical displacement, and the 95% prediction interval of each metamodel is considered. A scenario can be accepted without an additional FE run when the upper bound (Upper95) lies strictly below $\Delta_{\text{lim}}$; it should be rejected or redesigned when the lower bound (Lower95) exceeds $\Delta_{\text{lim}}$; and it warrants a targeted ADONIS reanalysis when the interval straddles this threshold. Because RF intervals are narrower and tend to under-cover, GB is preferable for direct compliance triage, whereas RF is suitable for rapid ranking and *what-if* exploration when an additional protection band is applied, for example by comparing $\text{Upper}95 + \delta$ against $\Delta_{\text{lim}}$ to mitigate overconfidence. In summary, we deliver a reproducible pipeline from SPT-derived stratigraphy to FE simulation, metamodel training, and decision-oriented uncertainty propagation, preserving traceability to the layered physics model and providing substantial savings in time and cost across design iterations, with a tool ready to support engineering decisions.

**Acknowledgements.** We thank the the Aeronautical Institute of Technology for their support in the research and development of this article,

**Authorship statement.** The authors hereby confirm that they are the sole liable persons responsible for the authorship of this work, and that all material that has been herein included as part of the present paper is either the property (and authorship) of the authors, or has the permission of the owners to be included here.

## References

[1] H. Adeli and C. Yeh. Perceptron learning in engineering design. *Computer-Aided Civil and Infrastructure Engineering*, vol. 4, n. 4, pp. 247–256, 1989.

[2] M. D. McKay, R. J. Beckman, and W. J. Conover. A comparison of three methods for selecting values of input variables in the analysis of output from a computer code. *Technometrics*, vol. 21, n. 2, pp. 239–245, 1979.

[3] D. W. Abueidda, Q. Lu, and S. Koric. Meshless physics-informed deep learning method for three-dimensional solid mechanics. *International Journal for Numerical Methods in Engineering*, vol. 122, n. 23, pp. 7182–7201, 2021.

[4] J. Bai, T. Rabczuk, A. Gupta, L. Alzubaidi, and Y. Gu. A physics-informed neural network technique based on a modified loss function for computational 2d and 3d solid mechanics. *Computational Mechanics*, vol. 71, n. 3, pp. 543–562, 2023.
[5] I. Yilmaz and H. Sendir. Correlation of schmidt hardness with unconfined compressive strength and young's modulus in gypsum from sivas (turkey). *Engineering Geology*, vol. 66, n. 3-4, pp. 211–219, 2002.
[6] C. Hellmich, H. A. Mang, and F.-J. Ulm. Hybrid method for quantification of stress states in shotcrete tunnel shells: Combination of 3d in-situ displacement measurements and thermochemoplastic material law. *Computers and Structures*, vol. 79, n. 21, pp. 2103–2115, 2001.
[7] R. Lackner, J. Macht, C. Hellmich, and H. A. Mang. Hybrid method for analysis of segmented shotcrete tunnel linings. *Journal of Geotechnical and Geoenvironmental Engineering*, vol. 128, n. 4, pp. 298–308, 2002.
[8] C. Xu, Z. Liu, B. T. Cao, G. Meschke, and X. Liu. Multifidelity operator learning for predicting displacement fields of tunnel linings under external loads. *IOP Conference Series: Earth and Environmental Science*, vol. 1333, 2024.
[9] Y. Zhang, J. Karlovšek, and X. Liu. Identification method for internal forces of segmental tunnel linings via the combination of laser scanning and hybrid structural analysis. *Sensors*, vol. 22, n. 6, pp. 2421, 2022.
[10] Z. Zhou, J. Zhang, and C. Gong. Hybrid semantic segmentation for tunnel lining cracks based on swin transformer and convolutional neural network. *Computer-Aided Civil and Infrastructure Engineering*, vol. 38, n. 17, pp. 2491–2510, 2023.
[11] G. Wang, Q. Fang, J. Wang, Q. Li, J. Chen, and Y. Liu. Estimation of load for tunnel lining in elastic soil using physics-informed neural network. *Computer-Aided Civil and Infrastructure Engineering*, vol. , 2024.
[12] A. T. Siacara, A. T. Beck, and J. Ji. Impact of random field simulations on fem-based earth slope reliability. *Geotechnical and Geological Engineering*, 2024.
[13] K. K. Phoon and F. H. Kulhawy. Characterization of geotechnical variability. *Canadian Geotechnical Journal*, vol. 36, n. 4, pp. 612–624, 1999.
[14] G. A. Fenton and D. V. Griffiths. *Risk Assessment in Geotechnical Engineering*. John Wiley & Sons, 2008.
[15] R. Kumar, D. Choudhury, and K. Bhargava. Determination of blast induced ground vibration equations for rocks using mechanical and geological properties. *Journal of Rock Mechanics and Geotechnical Engineering*, vol. 10, pp. 16–23, 2016.
[16] R. Kumar, K. Bhargava, and D. Choudhury. Correlations of uniaxial compressive strength of rock mass with conventional strength properties through random number generation. *International Journal of Geomechanics*, vol. 17, n. 2, pp. 06016021, 2017.
[17] K. Terzaghi and R. B. Peck. *Soil mechanics in engineering practice*. Wiley, New York, 2 edition, 1967.
[18] R. Kumar, D. Choudhury, and K. Bhargava. Response of shallow foundation in rocks subjected to underground blast loading using flac3d. *Disaster Advances*, vol. 7, n. 2, pp. 64–71, 2014.
[19] R. Kumar, D. Choudhury, and K. Bhargava. Simulation of rock subjected to underground blast using flac3d. In *Japanese Geotechnical Society Special Publication. In section 1. Characterization-rock and expansive soil. The 15th Asian Regional Conference on Soil Mechanics and Geotechnical Engineering*, volume 2, pp. 508–511, 2015.
[20] T. K. Ho. Random decision forests. In *Proceedings of 3rd International Conference on Document Analysis and Recognition*, volume 1, pp. 278–282 vol.1, 1995.